

Neural activity of orbitofrontal cortex contributes to control of waiting

Xiong Xiao,^{1,2} Hanfei Deng,^{1,2} Lei Wei,¹ Yanwang Huang¹ and Zuoren Wang¹

¹Institute of Neuroscience, State Key Laboratory of Neuroscience and CAS Center for Excellence in Brain Science and Intelligence Technology, Shanghai Institutes for Biological Sciences, University of Chinese Academy of Sciences, Shanghai 200031, China

²Graduate School of University of Chinese Academy of Sciences, Shanghai, China

Keywords: electrophysiology, optogenetics, orbitofrontal cortex, rat, waiting

Edited by John Foxe

Received 11 April 2016, revised 24 May 2016, accepted 20 June 2016

Abstract

The willingness to wait for delayed reward and information is of fundamental importance for deliberative behaviors. The orbitofrontal cortex (OFC) is thought to be a core component of the neural circuitry underlying the capacity to control waiting. However, the neural correlates of active waiting and the causal role of the OFC in the control of waiting still remain largely unknown. Here, we trained rats to perform a waiting task (waiting for a pseudorandom time to obtain the water reward), and recorded neuronal ensembles in the OFC throughout the task. We observed that subset OFC neurons exhibited ramping activities throughout the waiting process. Receiver operating characteristic analysis showed that neural activities during the waiting period even predicted the trial outcomes (patient vs. impatient) on a trial-by-trial basis. Furthermore, optogenetic activation of the OFC during the waiting period improved the waiting performance, but did not influence rats' movement to obtain the reward. Taken together, these findings reveal that the neural activity in the OFC contributes to the control of waiting.

Introduction

The willingness to resist an instant temptation and wait for a forthcoming reward is a characteristic of rationality (Reyna & Farley, 2006; McGuire & Kable, 2013). The control of waiting for delayed reward and information is disturbed in various disorders, including attention-deficit/hyperactivity disorder, drug addiction, self-control disorders and personality disorders (Knoch & Fehr, 2007; Pattij & Vanderschuren, 2008; Dalley *et al.*, 2011). However, how the brain exerts rational control over waiting remains to be fully understood.

Patients with damage to orbitofrontal cortex (OFC) tend to be more impatient (Berlin *et al.*, 2004), and functional imaging in humans has revealed that the degree of activation in lateral prefrontal areas (including OFC) is positively correlated with choosing larger delayed rewards over smaller immediate rewards (McClure *et al.*, 2007). Lesions of lateral/ventral OFC lead to increased impulsive choices in the delay discounting task (Mobini *et al.*, 2002; Rudebeck *et al.*, 2006; Mar *et al.*, 2011), and disrupts waiting-based confidence reports (Lak *et al.*, 2014). Prior neural recording studies have revealed that OFC plays roles in delay discounting independent of the encoding of absolute reward value (Roesch *et al.*, 2006), and executive functions related to reconciling cognitive signals during response conflict (Mansouri *et al.*, 2014; Bryden & Roesch, 2015).

Recent studies have shown that optogenetic activation of serotonin neurons in dorsal raphe nucleus (DRN) promotes waiting (Miyazaki *et al.*, 2014; Fonseca *et al.*, 2015), and DRN stimulations can modulate the neural activities of OFC (Zhou *et al.*, 2015). These lines of evidence implicate OFC in the control of waiting.

The underlying neurophysiological mechanisms of OFC in the control of waiting still remain elusive. Here, we trained rats to wait for a random delay to obtain the rewards, and recorded the neural activity of OFC during the task. We observed that OFC neurons encoded multiple phases of the waiting behavior, and exhibited mixed selectivity. Activities of subset OFC neurons even reflected the differential control of waiting, leading to distinct waiting outcomes. Moreover, lesion or inactivation of OFC impaired the waiting performance. Optogenetic activation improved the waiting performance, but did not inhibit motor or motivation.

Materials and methods

Subjects

Male Long-Evans rats ($n = 36$) weighing 250–300 g (approximately 8–10 weeks) were purchased from SLAC (China). Rats were maintained on a standard 12-h light–dark cycle and given food ad libitum, but were restricted from water to motivate them to work for the water reward. All animal care followed the institutional guidelines,

Correspondence: Zuoren Wang, as above.
E-mail: zuorenwang@ion.ac.cn

and the procedures were approved by the Animal Care and Use Committee of the Institute of Neuroscience, Shanghai Institutes for Biological Sciences, Chinese Academy of Sciences, China.

Behavioral paradigm and training

Behavior took place in a custom-designed training box inside a sound and light attenuating chamber (Anilab Software & Instruments, China). Each box contained a trigger nose port and a reward nose port. Each nose port had an infrared beam across the front (used to detect whether the rat's nose was in the port). Rats were trained using an automated training protocol. Rats went through three stages before performing the task as described in the results. The first stage was the habituation stage. Rats learned to poke the trigger nose port and then get the reward by poking the reward nose port. This stage lasted for only 1 h. The second stage was to train the rats to wait for short pseudo-randomly distributed durations (1.0, 1.5, 2.0, 2.5, 3.0 s), after which they got the reward by poking the reward port. This stage lasted for from 5 to 7 days. The third stage was to train the rats to wait for longer durations (2.0, 2.5, 3.0, 3.5, 4.0, 4.5, 5.0 s). In both the second and the third training stages, the rats did not need to respond very quickly to get the reward after the offset of the waiting tone. The goal of these two stages was to teach the rat that only poking the water port after the end of waiting tone can lead to the reward delivery, and premature poking would not lead to a reward delivery. In the final stage, the trial began with the rats' poking the trigger port, and a waiting tone with pseudo-random duration (2.0, 2.5, 3.0, 3.5, 4.0, 4.5, 5.0 s) followed immediately. Rats that waited to poke the water port until the end of the tone (within 2 s following the end of tone) were rewarded with water. Premature nose-poking of the water port led to the end of the tone without water delivery, and the trial was designated as an impatient trial. We used a uniformly distributed inter-trial interval (3–5 s). The trial of delayed nose-poking (> 2 s) was regarded as omission. As the omission trials only account for ~5% of total trials, we excluded these trials before data analysis.

Modeling rats' waiting time

We modeled rats' waiting time by Gaussian distribution. Modeling of rats' reaction time was based on the assumption that rats responded to the waiting tone by randomly choosing the time to poke the water port. The choosing of parameters for Gaussian distribution was based on the mean and standard deviation of rats' actual waiting time. The reaction time was defined as the time from the waiting tone offset to the water port entry. So only the 'patient' trials were selected for calculating the reaction time.

Microdrive implantation

Rats reached about 350 g before surgery. Surgical procedures followed guidelines for aseptic techniques. Rats were first briefly anesthetized with isoflurane, and then deeply anesthetized with pentobarbital sodium (0.08 g/kg, i.p.). A midline incision exposed the skull, which was subsequently thoroughly cleaned. Six skull screws were implanted at the periphery of the exposed skull to ensure stable recordings. Of the six screws, one screw was used as the reference, and another screw (above the cerebellum) was used as the ground for recording. A 2-mm craniotomy was drilled over the right OFC, and the dura mater was carefully resected.

Custom-made microdrives, consisting of 8 tetrodes made from ~12.5 μ m diameter Nichrome wires (Kanthal Palm Coast

electroplated with gold to an impedance of 300–400 k Ω at 1 KHz, were manufactured and implanted. Electrodes were implanted in ventrolateral portion of OFC (vlOFC) ($n = 5$; 3.2 mm anterior to bregma, 2.5 mm right of midline, and 3.6 mm ventral to dura). Dental acrylic was used to secure the electrodes to the skull and screws. The rats were given gentamicin (5 mg/kg, subcutaneous) and dexamethasone (2 mg/kg, subcutaneous) after surgery and recovered for at least one week.

Extracellular recording in freely moving rats

After surgery, rats were allowed to recover for at least one week before extracellular recording. Neurophysiology data was collected with a 64 channel Plexon Multichannel Acquisition Processor systems (Plexon). Signals from the electrode wires were first amplified 20 \times by an op-amp headstage, and then amplified ($\times 1000$), digitized at 40 kHz. Raw signal was filtered online (250–8000 Hz). Wires were screened for activity daily; if no activity was detected, the rat was removed from data collection and the electrode assembly was advanced 1/8–1/4 turn (37.5–75 μ m; each turn = 300 μ m). Otherwise a session was conducted and the electrode was advanced by 1/8 turn (37.5 μ m) after recording.

Isolation and classification of units

Single units were isolated offline by manually clustering spike waveform features (peak amplitude, energy and principle components) derived from the sampled waveforms using MClust 3.5 (written by A.D. Redish). Cluster quality was quantified by isolation distance and L-ratio. Only clusters with isolation distance > 15 and L-ratio < 0.2 were selected for further analysis (median isolation distance, 30.27; median L-ratio, 0.05).

Identification of neuronal response type

Neurons which showed significantly phasic increase in firing rate (0–1 s) before the trigger port entry (compared to firing rates during 1–1.5 s before trial initiation and 0.5–1 s after trial initiation; Wilcoxon signed-rank test, $P < 0.001$) were defined as 'start' cell. Neurons which showed significantly phasic increase in firing rate (0–1 s) immediately prior to the water port entry (compared to firing rates during period 1–1.5 s before water port entry; Wilcoxon signed-rank test, $P < 0.001$) were categorized as 'go' cell. Neurons with significantly higher firing rates during the waiting period were defined as 'hold' cell (compared to firing rates during period 1–1.5 s before water port entry; Wilcoxon signed-rank test, $P < 0.001$). Session-averaged neural responses were identified as having positive or negative ramping characteristics if they exhibited a significantly positive or negative linear regression coefficient (Pearson's $R > 0.5$ or $R < -0.5$ and $P < 0.05$) along the waiting period.

Peri-event time histograms and principal component analysis

A mean spike density function was constructed for each neuron by applying a Gaussian kernel ($\sigma = 50$ ms) to each spike. All of the peri-event time histograms (PETHs) were calculated in 50-ms time bins. The normalized (z-scored) firing rate was obtained by subtracting the mean and dividing by the standard deviation across trials. The temporally scaled PETH consisting of three time windows was constructed by aligning trials both to the waiting tone onset and to water port entry (or waiting tone offset). The first window was from –2 to 1 s by aligning trials to the waiting tone onset. The second

window (middle waiting period) was from 1 s after the waiting tone onset to 1 s before the water port entry (or waiting tone offset). The neural activity during this period was fitted to 20 equally spaced points for each trial, so that trials with different durations had the same number of time points. The third window is from -1 to 2 s, with the trials aligned to the water port entry (or waiting tone offset). For each neuron, the three windows were joined together as temporally scaled PETHs. To visualize the population neural activity dynamics, principal component analysis (PCA) was applied to the matrix of PETHs for all neurons (rows, neurons; columns, normalized firing rate). We randomly selected 100 neurons to calculate the PCAs (bootstrap for 100 times). This procedure reduced dimensionality while still retaining the maximum variance (Chapin & Nicollelis, 1999; Rabinovich *et al.*, 2008). To calculate the population trajectory distance between patient and impatients trials, we applied the first 30 principal components (PCs) (representing over 97% variance). The Euclidian distance of the trajectories for the 30 PCs was calculated for each time bin ($bin = 50$ ms). The period from 2 s to 1 s prior to the waiting tone onset was used as the baseline. Confidence interval of 95% was used to calculate statistical significance from baseline.

Correlation between neurons' activated duration with animals' waiting time

To link the duration of 'hold' cells' activation to animals' waiting time, we calculated the Pearson's correlation coefficient between them. Animals' waiting time was defined as the period from the waiting tone onset to water port entry. The duration of a 'hold' cell's activation was determined as the period when this cell's firing rate during waiting was significantly higher ($>\text{mean} + 3\text{*SD}$) than the baseline activity (0–2 s before the waiting tone onset) for each trial.

Decoding neural responses

To assess whether neural responses of OFC neurons reflected trial outcomes, we performed a population classification analysis. The goal of this decoding analysis was to train a trial-by-trial classifier to discriminate patient vs. impatients trials (Raposo *et al.*, 2014; Brincat & Miller, 2015). For a neuron to be included in this analysis, we required at least 20 trials for each trial outcome. As most neurons were not recorded simultaneously, we therefore constructed 'pseudo-trials' by choosing random trials for each neuron. Pseudo-trials were assembled by randomly selecting 20 trials (10 patient trials, 10 impatients trials) for training the classifier and 20 distinct trials (10 patient trials, 10 impatients trials) for testing. Then we used the linear support vector machine (SVM) to train the classifier for trial outcomes. The predictive accuracies were averaged across 100 random trial selections.

Receiver operating characteristics analysis

To examine the correlation between neuron activity and behavioral outcome, we calculated the outcome preference index (OPI) for each neuron–outcome pair. For each neuron, trials were classified into two groups according to the trial outcome (i.e., 'patient' vs. 'impatient'). Receiver operating characteristic (ROC) curves were calculated by comparing the distribution of firing rates across trials in 100 bins on patient and impatients trials, respectively. The area under ROC curve (auROC) was used to quantify the relationship between neural responses and trial outcomes (Britten *et al.*, 1996; Kepes

et al., 2008). The statistical significance of auROC (relative to the chance level of 0.5) was determined by permutation test (1000 times). OPI was used to scale the auROC so that it ranges from -1 to 1 with the sign denoting whether a neuron was activated or suppressed on patient trials (Kepes *et al.*, 2008; Cohen *et al.*, 2012, 2015):

$$\text{OPI} = 2 * (\text{auROC} - 0.5)$$

OPI = 1: perfect discriminability (always firing more on patient trials), OPI = 0: no discriminability (no difference between patient and impatients trials), OPI = -1: perfect discriminability (always firing more on impatients trials).

Virus construction and packaging

Recombinant adeno-associated virus (AAV) vectors were serotyped with AAV9 coat proteins and packaged by Neuron Biotech (China). Viral titers were 2×10^{12} particles/mL for AAV9-hSyn-ChR2 (H134R)-mCherry, and 4×10^{12} particles/mL for AAV9-hSyn-mCherry.

Stereotaxic virus injection and optical fiber implantation

Rats were prepared for surgery similar as the procedures described in tetrode implanting. A midline incision exposed the skull, and craniotomies were made bilaterally above the OFC. Four skull screws were attached on the skull. Virus was injected with a Pico III system (Parker Hannifin). 1 μL injections was delivered to each hemisphere at AP 3.2 mm, ML 2.5 mm, DV 3.8 mm for a total of 2 μL per rat. After each injection the needle was left in place for 15 min and then slowly withdrawn. Two optical fibers (200 μm in diameter, 0.37 NA, 6 mm in length) targeting the OFC were lowered and bilaterally implanted 300 μm above the injection sites of virus. Dental acrylic was used for structural support. The virus was allowed for at least two months to express.

Laser delivery

As to the optogenetic manipulation experiment, the laser power was checked before the testing to confirm that the optic fibers were intact. The fiber optic cable was attached before the testing, and an optical commutator (Doric Lenses, Canada) was used for unrestricted rotation. Optical stimulation was provided with a 473 nm diode pumped solid state laser (50 mW; Shanghai Laser & Optics Century, China) and controlled by the custom controlling device. The OFC activation experiments used 5 mW light at tips of fibers. The laser-on and laser-off trials were randomly interleaved. On laser-on trials, the 473 nm laser was turned on continuously during the waiting tone delivery period (15 ms pulse width, 20 Hz).

In vitro electrophysiology

For *in vitro* whole-cell recording, rats ($n = 2$) were first bilaterally injected with AAV9-hSyn-ChR2-mCherry into OFC (AP 3.2 mm, ML 2.5 mm, DV 3.8 mm; 1 μL for each hemisphere). After 2 months of recovery, the rats were deeply anesthetized with pentobarbital sodium (0.08 g/kg, i.p.) and intracardially perfused with ~100 mL ice-cold oxygenated artificial cerebrospinal fluid (aCSF) within 5 min. The aCSF for perfusion contained the following (in mM): NaCl 125, KCl 2.5, NaH₂PO₄ 1.3, MgCl₂ 1.3, CaCl₂ 2, NaHCO₃ 25 and glucose 20, bubbled with 95% O₂/5% CO₂. All

reagents were purchased from Sigma-Aldrich. After perfusion, brains were quickly removed and placed in ice-cold oxygenated aCSF. Coronal sections (350 µm) were prepared in aCSF using a Leica Vibratome 3000 microslicer. After slicing, brain slices were allowed to recover in a submersion holding chamber with solution containing (in mm) N-methyl-D-glucamin 110, HCl 110, KCl 2.5, NaH₂PO₄ 1.2, MgSO₄ 10, CaCl₂ 0.5, NaHCO₃ 25 and glucose 25, bubbled with 95% O₂/5% CO₂ for 15 min at 37 °C and a further 45 min in aCSF at 25–28 °C before recordings. ChR2-expression neurons in OFC were recognized based on the expression of mCherry fluorescence in somata. The internal solution within whole-cell recording pipettes (4–7 MΩ) contained the following (in mm): K-gluconate 130, HEPES 10, EGTA 0.6, KCl 5, Na₂ATP 3, Na₃GTP 0.3, MgCl₂ 4 and Na₂phosphocreatine 10 (pH 7.4). Recordings were performed using a MultiClamp700B amplifier (Molecular Devices). For voltage-clamp recordings, neurons were held at -60 mV. The data were low-pass filtered at 2 kHz and acquired at 10 kHz with a Digidata 1440A digitizer (Molecular Devices). The data were acquired and analyzed using Clampfit 10.0 software (Molecular Devices). For light stimulation, ChR2 was activated using a LED light source (10 mW power, 1 ms pulse width, 1 s duration).

Pharmacological lesion and inactivation

After about two months of training and the success rate reached a relatively stable high level (~50%), rats were randomly selected to be in one of two groups: OFC lesion group and sham lesion group. The experimenter was not blinded to group allocation. As to the OFC lesion group, rats were bilaterally injected with ibotenic acid (0.5 µL, 10 mg/mL, Sigma) in OFC. Sham lesion rats were bilaterally infused with saline of the same volume. Rats were housed individually after surgery. After five days of recovery, rats were water-deprived and tested for waiting performance. Behavioral performance for the first five days after recovery was used for the behavioral analysis.

Pharmacological inactivation was achieved via localized injection of GABA-A receptor agonist muscimol (Sigma). First, rats implanted with guide cannulae were lightly anesthetized induced by isoflurane. Then two cannulae (RWD Life Science, China), connected to two 5-µL syringes (Hamilton microliter syringe), were inserted into each previously implanted guide cannula. Internal cannulae extended 0.5 mm below the guide. Muscimol was infused into OFC with a concentration of 1.0 mg/mL and a volume of 0.5 µL per site. To confirm that the fluid was flowing, we monitored the injections by observing the movement of a small air bubble in the tubing. After infusions were completed, the cannulae were left in the brain for 3 more minutes to allow diffusion of muscimol. Rats were removed from anesthesia and returned to cages for 15 min before beginning behavioral testing. The same procedure was conducted for the control experiment in the same animals in other days, in which muscimol was replaced with saline (0.9%; 0.5 µL). It should be noted that each rat was tested in both muscimol and vehicle conditions, and the treatment order was counter-balanced.

Histology and immunohistochemistry

Before sacrifice for histology rats were deeply anesthetized with pentobarbital sodium and electric current passed through all electrodes (for each tetrode, 50 µA for 10 s) to make electrolytic lesions for anatomical localization. Rats were then transcardially perfused with ice-cold 4% paraformaldehyde (PFA) in PBS (pH 7.4). Brains were fixed in PFA overnight and then transferred to 30% sucrose in

PBS to equilibrate for at least 3 days. 60 µm coronal sections were cut on a freezing microtome. The Nissl staining was performed on sections to determine the electrode location.

For immunohistochemistry, sections were washed with PBS and incubated for 10 min in PBST (PBS with 0.3% Triton X-100). Sections were then washed in PBS and incubated in 4', 6-diamidino-2-phenylindole (DAPI, 1:1000) for 20 min, then washed again and mounted on slides with 75% Glycerine. Images were acquired using a Nikon confocal scanning laser microscope with a 10× or 20× air objective.

Data analysis

Analyses of neural data and behavioral data were conducted using custom written Matlab (Mathworks) scripts, open source toolboxes (including MClust, FieldTrip and Chronux), Neuroexplorer (Nex Technologies) and Prism 6 (GraphPad Software). All data are expressed as mean ± SEM, unless stated otherwise. Group differences in behavior were determined using Student's *t*-test, or two-way ANOVA followed by Bonferroni post hoc correction. To determine the statistical significance in electrophysiological data (firing rate, peak time and peak), we applied nonparametric Wilcoxon rank-sum test or Wilcoxon signed-rank test. To determine the significance of the difference in two distributions, we used Kolmogorov-Smirnov test. All comparisons for two-group were two-sided.

Results

Behavior

Adult rats were trained to perform a waiting task, similar to previous waiting tasks (Miyazaki *et al.*, 2014; Fonseca *et al.*, 2015). In our task, a water-restricted rat self-initiated a trial by poking its snout into a trigger port. After trial initiation, a tone with a pseudo-random duration (2–5 s, uniformly distributed) was presented to signify the waiting period. Rats were rewarded with water when they waited to poke the water port until the offset of the tone (patient trial), whereas premature nose-poking of the water port led to the end of the tone without water delivery (impatient trial) (Fig. 1A). We observed that the waiting time was much longer on patient trials than impatient trials (Fig. 1B; Kolmogorov-Smirnov, *P* < 0.001). To examine whether rats acquired the behavioral rule rather than acted by randomly poking the water port, we compared the distribution of rats' actual reaction time with time generated by random modeling (Gaussian distribution). We found that on the majority of trials rats responded by poking the water port ~250 ms after the waiting tone offset, whereas there was no such pattern in the model (Fig. 1C). These results indicate that the rats' responses were not random behaviors. In addition, the success rate of waiting increased gradually as the training preceded (Fig. 1D), another line of evidence supporting that rats were acquiring the rule. In the early stages, rats were relatively more impatient and responded prematurely more often, whereas in the later stages, rats learned to wait for longer durations (Fig. 1D). In addition, rats generally showed higher success rates on trials with shorter waits, but tended to give up on trials with longer waits.

Heterogeneous neural activities of OFC during the waiting task

To explore the neural correlates of the waiting behavior, we recorded spiking activity of OFC neurons using chronically movable

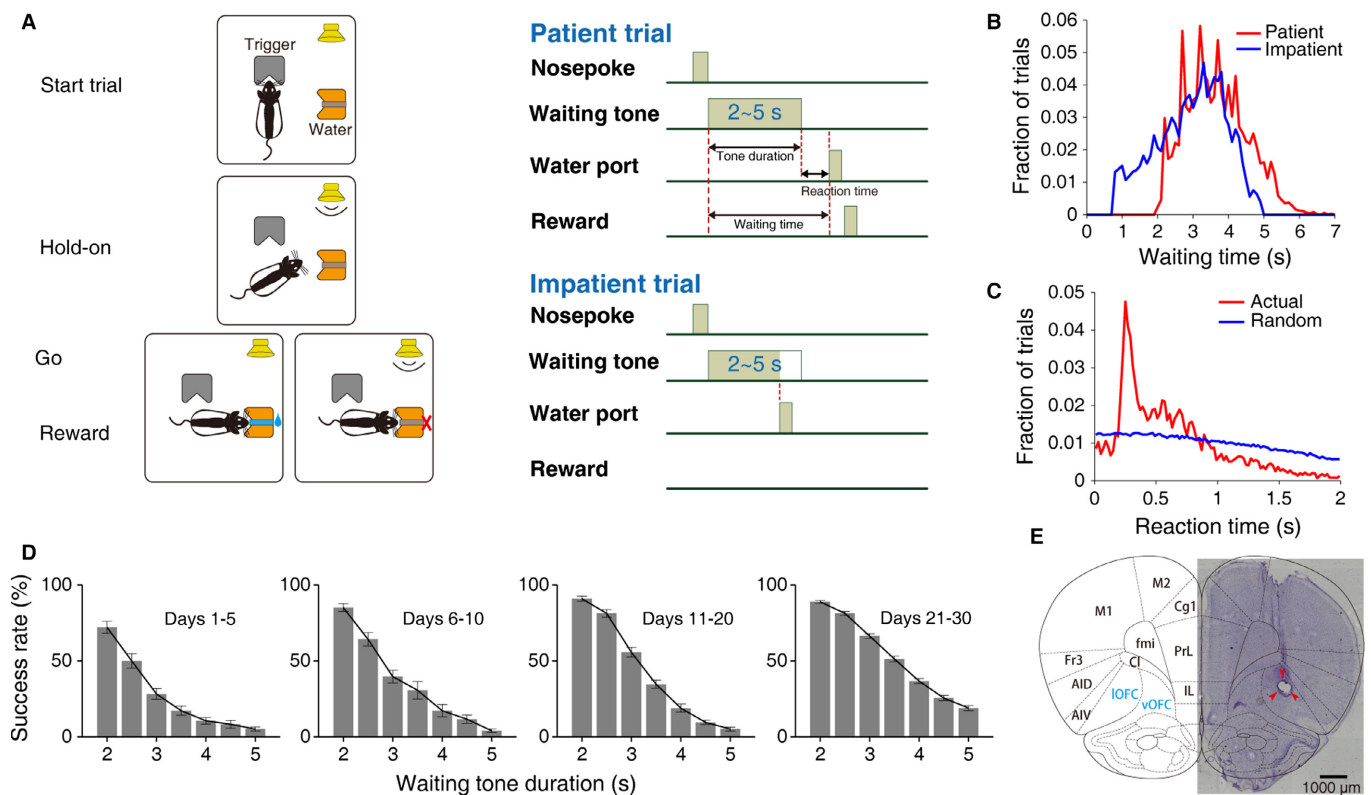


FIG. 1. Behavioral task, performance and recording sites. (A) (Left) Schematic diagrams for the waiting task. (Right) Timelines of patient and impatient trials. (B) Distribution of rats' actual waiting time for patient (red) and impatient (blue) trials (mean = 3.4 s, SD = 0.97 s; data pooled from 9 rats). Waiting time is defined as the period from the waiting tone onset to the water port entry. (C) Distribution of rats' actual reaction time (red line; data pooled from 9 rats) and the reaction time produced by Gaussian modeling (blue line; $n = 1000$ times). Reaction time is defined as the delay from the waiting tone offset to the water port entry only on patient trials. (D) Success rates for each duration of waiting tone (2–5 s) with training. Error bars represent SEM. (E) Anatomical location of the recording sites. Electrolytic lesion and Nissl-stained coronal section from a representative rat. The recording site is denoted by red arrowheads. IOFC, lateral OFC; vOFC, ventral OFC. Scale bar, 1000 μ m.

tetrodes in rats performing the waiting task. A total of 903 well-isolated single units were acquired from five rats. The recording sites were confirmed by electrolytic lesions and histology after completion of electrophysiological data collection (Fig. 1E; see also Fig. S1).

In order to more clearly depict the task, we divided the task into four consecutive phases based on key events: ‘start’, ‘hold’, ‘go’ and ‘outcome’ phases. We then analyzed the neural activity related to the four phases of this task. Neurons were defined as ‘start’, ‘hold’, ‘go’ and ‘outcome’ cells on the basis of their response profile (Fig. 2A–D). During the waiting task, OFC neurons displayed a wide variety of firing patterns that were associated with different phases of the task (Fig. 2A–D). Some neurons showed mixed selectivity, responsive to multiple behavioral events (Fig. 2E–G). In total, ‘start’, ‘hold’, ‘go’ and ‘outcome’ cells accounted for 14%, 19%, 17% and 64% of the population, respectively (Fig. 2H), and 31% (281/903) showed mixed selectivity, responsive to multiple behavioral events.

Population neural dynamics of OFC during the waiting task

To visualize the population neural activity of OFC neurons during the task, we constructed temporally scaled PETHs for each neuron, and averaged them across neurons (Fig. 3A). The average PETH showed that many neurons were phasically activated prior to the waiting tone onset or the water port entry. Notably, the population neural activity exhibited the ramping-up trend throughout the waiting

period. As the waiting time elapsed, OFC neurons were recruited gradually into different phases of the task (Fig. 3B). To explore the dynamics of the population neural activity throughout the task, we performed a PCA of population PETHs (Fig. 3C, left), and quantified the trajectory distance between patient and impatient trials (Fig. 3C, right) (Liu *et al.*, 2014). The OFC has long been known to signal value and play an important role in outcome-guided behavior (Padoa-Schioppa & Assad, 2006; Schoenbaum *et al.*, 2011; Jones *et al.*, 2012). Consistently, the Euclidean distance between the PCs on patient and impatient trials was the largest when the outcome was revealed (after the water port entry). Moreover, it should be noted that the Euclidean distance between the PCs on patient and impatient trials was much larger than the baseline even prior to the water port entry (Fig. 3C, right), indicating differential population activities that were predictive of patient/impatient responses.

We next asked whether the firing activity of OFC neurons could predict trial outcomes. First we performed population decoding using the linear support vector machine method. The decoding accuracy during the waiting period was significantly higher than chance level (50%) even before the water port entry (Fig. 3D). Next, to further explore the link between neural activity of different types of cells and trial outcomes on the trial-by-trial basis, we applied a ROC analysis to these cells (Fig. 3E–G). We observed that more ‘hold’ and ‘go’ cells fired at significantly higher rates on impatient trials than on patient trials (43/172 and 31/157 for impatient trials vs. 4/172 and 9/157 for patient trials; Fig. 3G, middle and right). However, the population of ‘start’ cells exhibited no bias toward

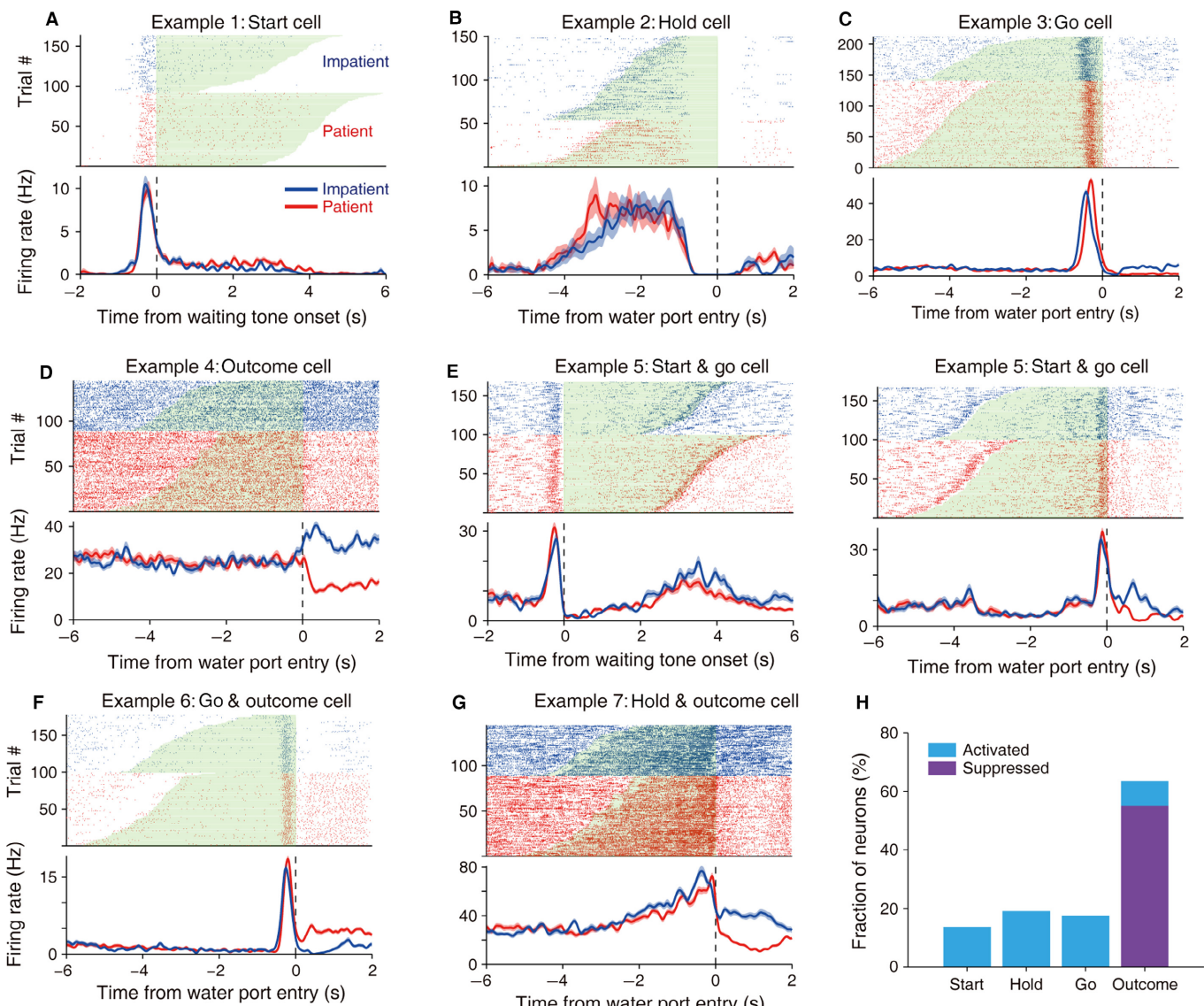


Fig. 2. Example OFC neurons responding to different behavioral events. (A–D) Example cells responding to the ‘start’ (A), ‘hold’ (B), ‘go’ (C) and ‘outcome’ (D) phases of the task. (Upper) Raster plot indicates spike trains, with each row corresponding to a single trial and each tick mark to a single spike. Red, patient trial; blue impatient trial. Green shading indicates the waiting period (from waiting tone onset to water port entry). Trials are sorted according to the waiting time. (Lower) PETH calculated by averaging the firing rates across trials. The mean \pm SEM are plotted for all PETHs. (E) Example of a neuron with ‘start’ and ‘go’ activities. For the same cell, trials are aligned to the waiting tone onset (left) and water port entry (right), respectively. (F) Example of a neuron with ‘go’ and ‘outcome’ activities. (G) Example of a neuron with ‘hold’ and ‘outcome’ activities. (H) Fraction of neurons responding to different phases of the task. Purple, activity suppressed; blue, activity activated.

impatient trials (7/172 for impatient trials vs. 8/172 for patient trials; Fig. 3G, left).

To test whether the persistent activity was due to the auditory tone, we exposed rats to the tone (2–5 s, same as the waiting tone in the waiting task) after rats freely consumed water for 30 min, and observed that OFC neurons were barely responsive to the tone when rats were not in the active state of waiting (Fig. S2A). Furthermore, we applied the PCA to the PETHs aligned to the waiting tone onset and offset (Fig. S2B). We observed that the distance became even larger before the tone offset, although tone stimuli were identical for patient and impatient trials (Fig. S2C). These results show that the differential neural activity before the water port entry was probably due to internal brain states, rather than an effect of waiting tone delivery.

Neural correlates of waiting

During the waiting period, some ‘hold’ cells showed relatively stable firing activity, whereas others exhibited ‘ramping’ activity as waiting proceeded. The ramping neural activities were identified in session averages by linear regression (Howe *et al.*, 2013). Cells were categorized according to the ramping rate calculated by linear regression (Pearson’s $R > 0.5$, $P < 0.05$ for ‘ramp-up’ cell; $R < -0.5$, $P < 0.05$ for ‘ramp-down’ cell; $P > 0.05$ for ‘non-ramp’ cell). Figure 4A shows an example of a ‘hold’ cell that exhibited a gradual increase in firing rates that began at the onset of the trial and ended immediately prior to the water port entry (Fig. 4B, Pearson’s $R = 0.94$, $P < 0.001$). In addition, the activated duration of this neuron correlated significantly with the rat’s

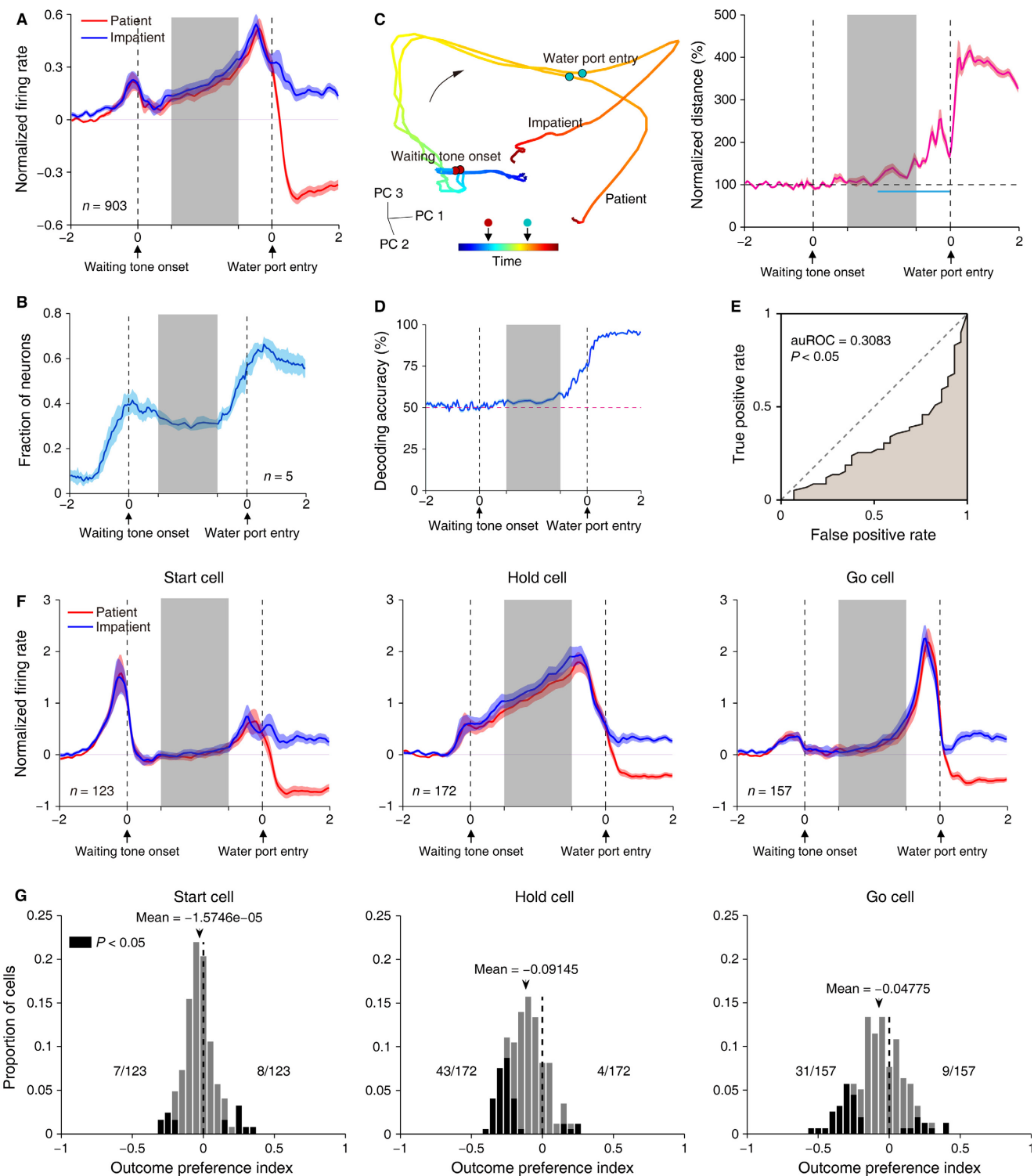


FIG. 3. Population activity of OFC neurons during the task. (A) Average normalized PETHs across all neurons on patient and impatient trials. Gray shading indicates the temporally scaled middle waiting period. (B) Average fraction of neurons responsive during the waiting task (bin = 50 ms) across rats ($n = 5$ rats). The neural activity from -2 to -1 s relative to the waiting tone onset was used as the baseline. For each neuron in each time bin, the responsiveness was evaluated by comparing its activity to the baseline activity on all trials (Wilcoxon signed-rank test, $P < 0.001$). Blue shading indicates SEM across rats. (C) Visualization of population neural activity by PCA. (Left) Neural responses on patient and impatient trials are projected onto the first three principal components. Red dot denotes waiting tone onset; cyan dot denotes water port entry. (Right) Normalized Euclidean distance of the principal components of population responses between patient and impatient trials. Orange shading indicates the 95% confidence interval from 100 bootstrap replicates. Blue line indicates the period with larger Euclidean distance than the baseline during waiting. (D) Population decoding accuracy of OFC neurons using the linear SVM method. (E) Example cell with negative outcome preference. The statistical significance was evaluated by permutation test ($n = 1000$). (F) Average PETHs of ‘start’ ($n = 123$), ‘hold’ ($n = 172$) and ‘go’ ($n = 157$) cells on patient and impatient trials. (G) Outcome preference for the ‘start’, ‘hold’ and ‘go’ cells during the trial initiation, holding, and going period, respectively. Outcome preference index is calculated by ROC analysis. Black bars indicate significant selectivity (1000 replicates of the permutation test, $P < 0.05$); gray bars indicate no significance ($P > 0.05$).

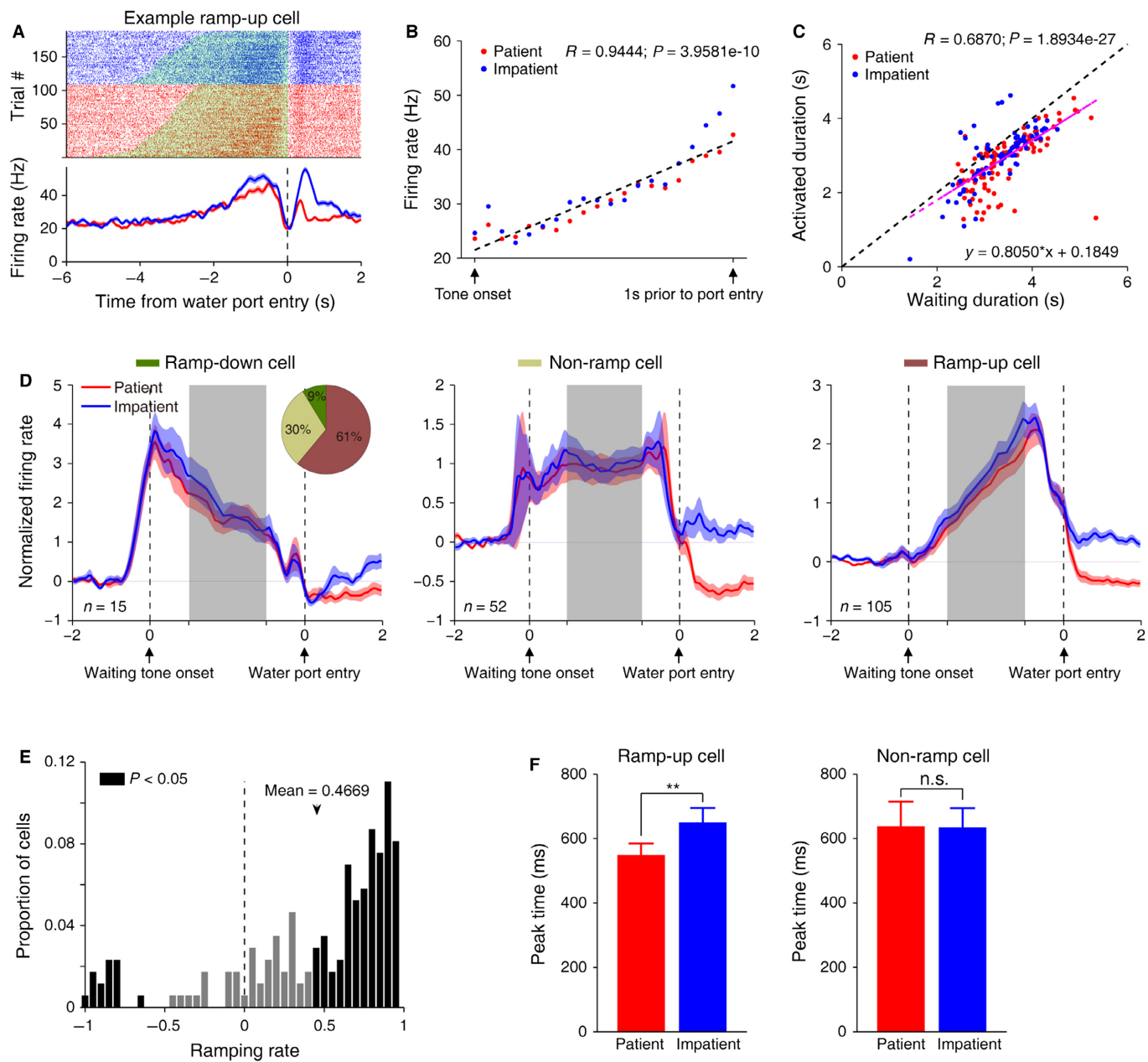


FIG. 4. ‘Hold’ cells correlate with waiting behavior. (A) Example of a ‘ramp-up’ cell, with spiking activity that increased with waiting. Green shading represents the waiting period. (B) The firing rate of the cell in (A) increased with the relative time of the waiting period. The time from waiting tone onset to 1 s before water port entry was fitted to 20 equally spaced time points for each trial. Dashed line represents the linearly regressed line. (C) Correlation between activated duration of the cell in (A) and animal’s actual waiting time. Pink line represents the linearly regressed line. Activated duration was defined as the time when this cell’s firing rate during waiting was significantly higher ($>\text{mean} + 3\text{SD}$) than the baseline activity (0–2 s before the waiting tone onset) for each trial. (D) Average normalized PETHs of ‘ramp-down’, ‘non-ramp’ and ‘ramp-up’ cells. Left, ‘ramp-down’ cells; inset is the proportion of ‘ramp-down’ ($n = 15$), ‘non-ramp’ ($n = 52$) and ‘ramp-up’ cells ($n = 105$). Middle, ‘non-ramp’ cells. Right, ‘ramp-up’ cells. Gray shading indicates the temporally scaled middle waiting period. (E) Distribution of the linearly regressed coefficient (Pearson’s R value). Arrowhead denotes the mean R value. Black bars indicate significance (Pearson’s $P < 0.05$); gray bars indicate no significance (Pearson’s $P > 0.05$). (F) (Left) Average peak time to water port entry for ‘ramp-up’ cells on patient and impatient trials (Wilcoxon signed-rank test, $**P < 0.01$). Peak time was defined as the time (relative to the water port entry) that a neuron’s firing rate decreased most significantly (the minimum of the first derivative). (Right) Average peak time to water port entry for ‘non-ramp’ cells on patient and impatient trials (Wilcoxon signed-rank test, $P = 0.6$; n.s., non-significant).

actual behavioral hold duration (Fig. 4C, Pearson’s $R = 0.69$, $P < 0.001$).

Over half of ‘hold’ cells (61%, 105/172) exhibited ramping-up spiking activity during waiting, and a smaller fraction (9%, 15/172) of ‘hold’ neurons showed steady decrease in firing activity (ramping-down) (Fig. 4D and E). The firing rates of ‘ramp-up’ cells began

to decrease earlier on impatient trials than patient trials (Fig. 4F, left; 549 ± 36 ms for patient trials vs. 650 ± 45 ms for impatient trials, mean \pm SEM; Wilcoxon signed-rank test, $P = 0.007$), whereas the firing activity of ‘non-ramp’ cells did not show such difference (Fig. 4F, right; Wilcoxon signed-rank test, $P = 0.6$). Together, the neural activities of ‘hold’ cells correlated well with

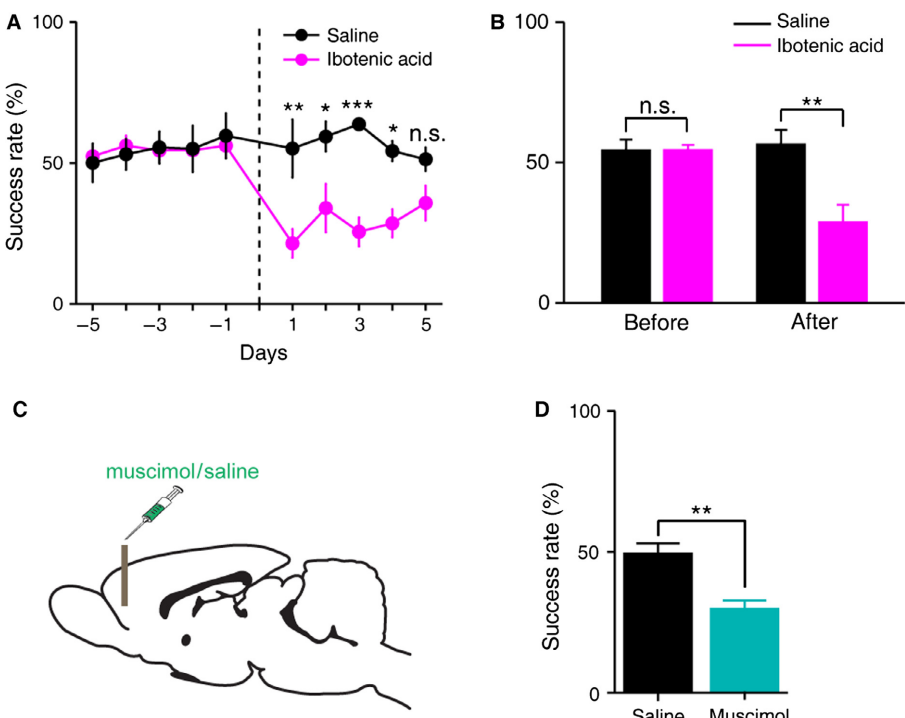


FIG. 5. Lesion or inactivation of OFC impairs the waiting performance. (A) Waiting success rate for five consecutive sessions before and after ibotenic acid (pink; $n = 6$ rats) or vehicle (black; $n = 3$ rats) injection (two-way ANOVA, group \times time interaction, $F_{9,63} = 6.17$, $P < 0.001$; days 1–5, $P = 0.0014$, 0.0331, 0.0002, 0.0304, 0.6754; Bonferroni post hoc analysis). (B) Mean success rates for waiting before and after ibotenic acid or vehicle application (two-way ANOVA, group \times time interaction, $F_{1,7} = 9.72$, $P = 0.017$; Bonferroni post hoc analysis). (C) Schematic diagram showing the injection of muscimol or vehicle into OFC. We performed within-subjects matched comparison, counter-balanced for treatment order. (D) Mean success rates for waiting following muscimol (cyan) and vehicle (black) injection ($n = 6$ rats; Student's paired *t*-test, $P = 0.003$). n.s., non-significant, $P > 0.05$; * $P < 0.05$; ** $P < 0.01$; *** $P < 0.001$. Error bars represent SEM.

the waiting behavior, and the distinction in neural activities may reflect the differential control of waiting.

Lesion or inactivation of OFC impairs waiting performance

Prior work suggests that OFC is essential for the control of impulsivity and waiting confidence (Winstanley *et al.*, 2004; Mar *et al.*, 2011; Lak *et al.*, 2014). To confirm the necessity for OFC in the control of waiting, we chose to apply ibotenic acid, an excitotoxic agent, to make lesions in OFC. Rats were first trained in the waiting task. After reaching criterion performance levels (~50%), rats were tested for an additional five consecutive days to acquire the baseline performance. Then we injected ibotenic acid (10 mg/mL, Sigma) bilaterally into OFC of experimental rats ($n = 6$, lesion group), and saline in control rats ($n = 3$, sham-lesion group). After five days of

recovery, we examined the waiting performance of rats in the lesion and sham-lesion groups. OFC lesion significantly affected the waiting performance ($56.77 \pm 4.68\%$ for saline vs. $29.08 \pm 5.09\%$ for ibotenic acid, mean \pm SEM; two-way ANOVA, Bonferroni post hoc, $P = 0.004$; Fig. 5A and B). The gradual recovery of performance after lesion may be due to compensation by other prefrontal areas (Zelikowsky *et al.*, 2013).

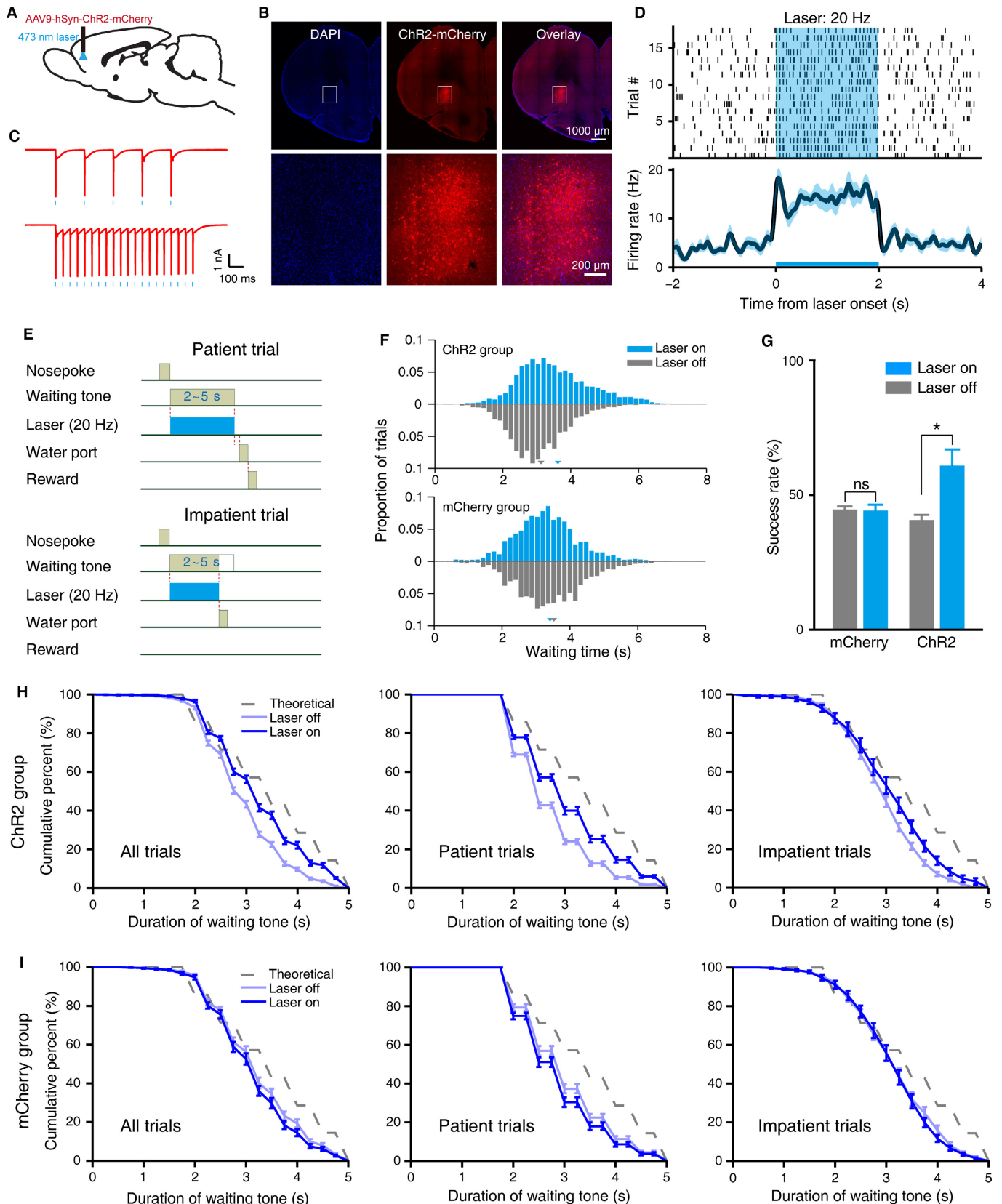
Next, we tested whether transient inactivation of OFC could also impair the waiting performance. When rats reached criterion performance levels (~50%), they were bilaterally implanted with cannulae in OFC. Following recovery, rats ($n = 6$) received an intra-OFC infusion of either the GABA-A agonist muscimol (1.0 mg/mL, Sigma) for suppressing neural activity or saline as the control (Fig. 5C). When muscimol was administered into OFC, the waiting performance decreased significantly (Fig. 5D, $49.72 \pm 3.33\%$ for

FIG. 6. Optogenetic activation of OFC improves waiting performance. (A) Schematic of the injection of AAV and implantation of optical fiber into OFC. After reaching criterion performance levels, rats were injected with AAV9-hSyn-ChR2-mCherry or AAV9-hSyn-mCherry and implanted with optical fibers bilaterally in OFC. (B) (Upper) Visualization of ChR2-mCherry expression in OFC (DAPI, blue; ChR2-mCherry, red). Scale bar, 1000 μ m. (Lower) The boxed areas in the upper panels are enlarged and shown in the lower panels. Scale bar, 200 μ m. (C) Recordings from brain slices of ChR2-expressing rats show precise neuronal activation with blue light pulses (pulse duration = 1 ms) at 5 and 20 Hz, respectively. (D) An example neuron recorded *in vivo* in a ChR2-expressing rat increased its firing rate upon laser stimulation. (Upper) Raster plot of spiking activity. Blue shading indicates the period of laser delivery (473 nm, 20 Hz, 5 mW). (Lower) Average firing rate across trials. Blue shading indicates SEM, and blue horizontal bar indicates the period of laser delivery. (E) Protocol of laser delivery during the waiting task. The laser stimulation always coincided with the waiting tone. (F) In the ChR2 group (upper), laser illumination significantly prolonged the waiting time (Kolmogorov–Smirnov test, $P < 0.001$). In the mCherry group (lower), laser illumination did not increase the waiting time. Arrowhead denotes the mean waiting time. (G) Success rates of waiting in the ChR2 and mCherry groups. Laser illumination significantly improved the waiting performance in the ChR2 group ($n = 5$ rats; two-way ANOVA, group \times epoch interaction, $F_{1,8} = 7.3$, $P = 0.027$; Bonferroni post hoc analysis, $P = 0.011$), but not in the mCherry group ($n = 5$ rats; two-way ANOVA; Bonferroni post hoc, $P > 0.05$). (H) Cumulative percentage plots of waiting tone durations with and without laser delivery in the ChR2 group on all trials (left), patient trials (middle) and impatient trials (right). Dark blue line, laser on; light blue line, laser off; dashed gray line, the theoretical cumulative percentage of waiting tone durations if rats' success rate were 100%. (I) Cumulative percentage plot of waiting tone durations with and without laser delivery in the mCherry group on all trials (left), patient trials (middle) and impatient trials (right). Error bars represent SEM. * $P < 0.05$.

saline vs. $30.08 \pm 2.65\%$ for muscimol, mean \pm SEM; Student's paired t test, $P = 0.003$). These results show that OFC is necessary for the control of waiting.

Optogenetic activation of OFC improves waiting performance

To further examine the causal role of OFC in the control of waiting, we measured the behavioral effect of optogenetic activation of OFC



during waiting. We first expressed channelrhodopsin-2 (ChR2) in OFC using an adeno-associated viral vector serotype 9 (AAV9-hSyn-ChR2(H134R)-mCherry), and then implanted optical fibers bilaterally over OFC to allow for the delivery of laser (473 nm) (Fig. 6A and B). The control animals received the same viral vector but carrying hSyn-mCherry. To confirm the effectiveness of the optogenetic activation, we performed whole-cell patch-clamp recording in brain slice and *in vivo* recording by ‘optrodes’ (tetrodes coupled to the optical fiber). The illumination of OFC evoked spikes precisely time-locked to light pulses in brain slice (Fig. 6C), and significantly increased the firing rates of OFC neuron recorded in awake rats as well (Fig. 6D, Wilcoxon signed-rank test, $P < 0.001$). To examine whether optogenetic activation of OFC influenced waiting performance on a trial-by-trial basis, we activated OFC neural activity during the waiting period in an interleaved laser on/off design (Fig. 6E). Rats in the ChR2 group ($n = 5$ rats) showed significantly higher waiting performance and longer waiting time on laser-on trials than laser-off trials (two-way ANOVA, Bonferroni post hoc, $P = 0.011$), whereas those in the mCherry group did not ($n = 5$ rats; two-way ANOVA, Bonferroni post hoc, $P > 0.05$) (Fig. 6F and G). In the ChR2 group, rats showed longer waiting durations in the laser-on trials than laser-off trials (Fig. 6H). As a control in the mCherry group, the laser illumination did not significantly influence the waiting durations (Fig. 6I). To exclude the possibility that activation of OFC affected movement or the motivation for rats to drink water, we trained these rats to perform the control

task without the need to wait before poking the water port (Fig. 7A). Activation of OFC did not affect the response delay in this task (Fig. 7B–D), suggesting that OFC activation did not influence movement per se or the motivation to work for water.

Discussion

The control of waiting is essential for deliberative behavior. Recent studies have shown that the activation of DRN serotonin neurons contributes to waiting for delayed rewards (Miyazaki *et al.*, 2011, 2012, 2014; Fonseca *et al.*, 2015), and optogenetic activation of the lateral orbitofronto-striatal projection decreases compulsive behavior (Burguiere *et al.*, 2013). Here we explored the role of OFC, a region potentially downstream of DRN (McDannald, 2015; Zhou *et al.*, 2015) in a waiting task. This task is similar to previous waiting tasks (Miyazaki *et al.*, 2014; Fonseca *et al.*, 2015), in which all the rats had to do was to start a trial and wait to get the reward. The rats did not need to discriminate multiple stimuli or make different choices, and the constant reward size can minimize the involvement of economic decision-making processes. This task is different from the delay discounting task.

In our study, the lesion or inactivation of OFC impaired animals' control of waiting. Similarly, it has been reported that infusions of muscimol into the infralimbic but not the prelimbic cortex have increased rats' impulsivity (Murphy *et al.*, 2005, 2012). In addition, the medial and lateral OFC may play different roles in the control of

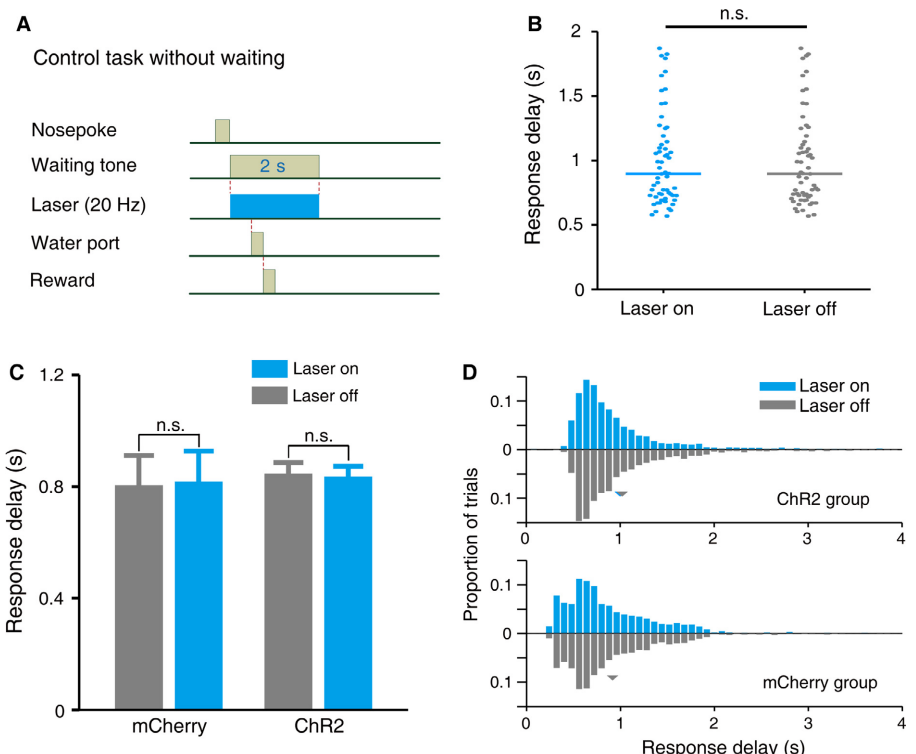


FIG. 7. Optogenetic activation of OFC does not influence movement. (A) Protocol of laser delivery during the control task without waiting. The rat self-initiates a trial by nose-poking the trigger port, which triggers an immediate tone and laser stimulation both lasting for 2 s. The rat was rewarded with water by poking the water port within 2 s. The laser stimulation always coincided with the waiting tone. (B) Example of a rat's response delay in the control task without need to wait on laser-on (blue) and laser-off (gray) trials (Student's *t* test, $P > 0.05$; n.s., non-significant). The response delay is defined as the time from the trigger port entry to the water port entry. (C) Average response delay across rats on laser-on and off trials in the ChR2 and mCherry group ($n = 5$ rats for each group; two-way ANOVA, group \times epoch interaction, $F_{1,8} = 0.6$, $P = 0.45$; Bonferroni post hoc analysis, $P > 0.05$; n.s., non-significant). (D) Distribution of response delay on laser-on and off trials. There was no significance in the distribution of response delay between laser-on and off trials in the ChR2 (Kolmogorov-Smirnov test, $P = 0.24$) and mCherry (Kolmogorov-Smirnov test, $P = 0.91$) groups ($n = 5$ rats for each group). Arrowhead denotes the mean response delay.

waiting (Mar *et al.*, 2011). This suggests that the higher cognitive control over impulsivity is a feature shared by some prefrontal areas, but not all prefrontal areas. Moreover, we observed that OFC neurons exhibited ramping activities throughout the waiting process. The ramping-up spiking activity of OFC resembles the ramping dopamine signal found in the striatum and the neural activity of secondary motor cortex (Howe *et al.*, 2013; Murakami *et al.*, 2014). This kind of ramping signal may represent the stronger reward expectation during waiting. Previous studies have shown that lesions of ventral striatum (nucleus accumbens) or hippocampus induce increased impulsive choices in the delay discounting tasks (Cardinal *et al.*, 2001; Mariano *et al.*, 2009; Abela & Chudasama, 2013). The OFC receives inputs from ventral tegmental area and hippocampus, and sends projections to the nucleus accumbens (Cavada *et al.*, 2000; Rempel-Clower, 2007; Wallis, 2007). The ventral tegmental area is a major midbrain region containing dopamine neurons, and sends projections to both the nucleus accumbens and OFC (Beier *et al.*, 2015; Menegas *et al.*, 2015). It is possible that the ramping dopamine signal observed in the nucleus accumbens arises from the ventral tegmental area, and the ramping neural activity of OFC may also come from the ventral tegmental area. Future study should be performed to investigate the origin of the ramping signal, and the downstream target of the ramping activity. Here we further examined whether the OFC neural dynamics reflected animals' internal state of waiting control. ROC analysis revealed that the spiking activities could predict trial outcomes even before the outcome reveal.

In our study, the optogenetic activation presumably increased the overall activity of OFC, and it remains unclear which types of optogenetically activated neurons contributed to the behavioral change. The optogenetic activation probably increased the persistent firing duration of 'hold' cells to prolong the control of waiting, although we cannot exclude the possible activation of 'go' cells. We propose possible explanations of the behavioral effect of optogenetics: (i) the firing of 'ramp-up' cells (accounting for 61% of the total 'hold' cells) ceased much earlier on impatient trials, and (ii) the optogenetic activation may postpone the cessation of persistent firing of 'hold' cells to prolong the 'holding' duration. That is, although the 'hold' cells tended to fire at a higher rate on impatient trials, the optogenetic activation increased the activated duration which contributed to the prolonged holding behavior.

It has been proposed over the past decades that a key function of OFC is inhibitory control. Some data show that OFC damage leads to deficits in response inhibition (Mobini *et al.*, 2002; Rudebeck *et al.*, 2006; Zeeb *et al.*, 2010); whereas other data show the opposite (Winstanley *et al.*, 2004; Mariano *et al.*, 2009; Abela & Chudasama, 2013). More recent studies have revealed that animals with OFC lesions can exhibit certain forms of inhibitory control as well as control animals do (Rudebeck *et al.*, 2013; Rudebeck & Murray, 2014; Stalnaker *et al.*, 2015). The inconsistency of the roles of OFC in response inhibition may arise from the following reasons. First of all, the OFC is comprised by different subregions in rats, including medial, lateral and ventral parts. Different subregions of the OFC may have different roles in the control of impulsivity. Mar *et al.* (2011) have shown that lateral OFC-lesioned rats showed increased impulsive choices, whereas medial OFC-lesioned rats showed decreased impulsive choices in the delay discounting task. The lesion of whole OFC may not induce observable behavioral effects on impulsivity. So, it is probably that the discrepancy between our findings and others' is due to the differences in the targeted subregions. Second, the behavioral paradigms used in different studies are quite diverse, and may involve some other factors besides response inhibition. Two commonly used behavioral paradigms are 5CSRTT

(Robbins, 2002) and delay discounting task (Cardinal *et al.*, 2001). The 5CSRTT is also used to study sustained attention (Bari *et al.*, 2008; Ljubojevic *et al.*, 2014), and the delay discounting task may involve the economic decision-making process under different temporal costs (small immediate rewards vs. larger delayed rewards) (Cardinal *et al.*, 2001; Roesch *et al.*, 2006, 2009, 2012; McGuire & Kable, 2012). Thus, utilization of distinct paradigms may involve different behavioral factors, eventually leading to differential interpretations.

The idea of inhibitory control also comes from some observations that lesion of OFC disrupts the reversal learning (Chudasama & Robbins, 2003; McAlonan & Brown, 2003; Schoenbaum *et al.*, 2003; Izquierdo & Murray, 2004). Such deficits may be due to the inability to inhibit some default response strategy. This indicates that OFC is required for the flexible representation of stimulus-outcome associations in the context of environmental change. However, it should be noted that OFC damage does not always lead to deficits in reversal learning (Kazama & Bachevalier, 2009; Rudebeck *et al.*, 2013). Moreover, the stimulus-outcome association is relatively stable in our waiting task. It is possible that the OFC provides state information and plays different roles in different contexts (Stalnaker *et al.*, 2015).

Here we observed that optogenetic activation of OFC during the waiting period significantly improved waiting performance (Fig. 6G), but did not affect the rats' movement or motivation to work (Fig. 7). This observation reveals that OFC does not control waiting through motor inhibition or suppression of motivation, suggesting OFC activation does not provide the signal of inhibitory control. This is consistent with the electrophysiological data that OFC does not carry a pure nondirectional inhibitory signal during response inhibition (Bryden & Roesch, 2015). Another possibility is that activation of OFC provides a rewarding signal to make rats wait longer, as activation of the human orbitofrontal cortex reflects the subjective pleasantness (Kringelbach *et al.*, 2003). However, this was disputed by the fact that optogenetic activation of OFC is not rewarding to rats in the optical self-stimulation experiments (Lucantonio *et al.*, 2014). We propose that activation of OFC increases the waiting time through enhancing the reward expectation. The optogenetic activation increased the activated duration which contributed to the prolonged holding behavior. Future investigations should delineate the specific roles of OFC activation leading to improved waiting performance.

Supporting Information

Additional supporting information can be found in the online version of this article:

Fig. S1 Extracellular recording.

Fig. S2 Effect of auditory tone on OFC neural activity.

Acknowledgements

This work was supported by the Chinese Academy of Sciences Strategic Priority Research Program (Grant No. XDB02040000). We thank Dr. L.N. Lin for help on tetrode drive manufacturing, Dr. Z.L. Qiu for help on AAV virus packaging, and L. Zhou for help in brain slice recording. We are grateful to X.W. Gu and Dr. Y. Gu for communication on data analysis. We also thank Drs. Y. Gu, T.M. Yang, M.C. Dorris and C.Y. Li for their critical comments on the manuscript.

Abbreviations

AAV, adeno-associated virus; ChR2, channelrhodopsin-2; DRN, dorsal raphe nucleus; OFC, orbitofrontal cortex; OPI, outcome preference index; PCA,

principal component analysis; PETH, peri-event time histogram; ROC, receiver operating characteristic; SVM, support vector machine.

References

- Abela, A.R. & Chudasama, Y. (2013) Dissociable contributions of the ventral hippocampus and orbitofrontal cortex to decision-making with a delayed or uncertain outcome. *Eur. J. Neurosci.*, **37**, 640–647.
- Bari, A., Dalley, J.W. & Robbins, T.W. (2008) The application of the 5-choice serial reaction time task for the assessment of visual attentional processes and impulse control in rats. *Nat. Protoc.*, **3**, 759–767.
- Beier, K.T., Steinberg, E.E., DeLoach, K.E., Xie, S., Miyamichi, K., Schwarz, L., Gao, X.J., Kremer, E.J. et al. (2015) Circuit architecture of VTA dopamine neurons revealed by systematic input-output mapping. *Cell*, **162**, 622–634.
- Berlin, H.A., Rolls, E.T. & Kischka, U. (2004) Impulsivity, time perception, emotion and reinforcement sensitivity in patients with orbitofrontal cortex lesions. *Brain*, **127**, 1108–1126.
- Brincat, S.L. & Miller, E.K. (2015) Frequency-specific hippocampal-prefrontal interactions during associative learning. *Nat. Neurosci.*, **18**, 576–581.
- Britten, K.H., Newsome, W.T., Shadlen, M.N., Celebrini, S. & Movshon, J.A. (1996) A relationship between behavioral choice and the visual responses of neurons in macaque MT. *Vis. Neurosci.*, **13**, 87–100.
- Bryden, D.W. & Roesch, M.R. (2015) Executive control signals in orbitofrontal cortex during response inhibition. *J. Neurosci.*, **35**, 3903–3914.
- Burguiere, E., Monteiro, P., Feng, G. & Graybiel, A.M. (2013) Optogenetic stimulation of lateral orbitofronto-striatal pathway suppresses compulsive behaviors. *Science*, **340**, 1243–1246.
- Cardinal, R.N., Pennicott, D.R., Sugathapala, C.L., Robbins, T.W. & Everitt, B.J. (2001) Impulsive choice induced in rats by lesions of the nucleus accumbens core. *Science*, **292**, 2499–2501.
- Cavada, C., Company, T., Tejedor, J., Cruz-Rizzolo, R.J. & Reinoso-Suarez, F. (2000) The anatomical connections of the macaque monkey orbitofrontal cortex. A review. *Cereb. Cortex*, **10**, 220–242.
- Chapin, J.K. & Nicolelis, M.A. (1999) Principal component analysis of neuronal ensemble activity reveals multidimensional somatosensory representations. *J. Neurosci. Meth.*, **94**, 121–140.
- Chudasama, Y. & Robbins, T.W. (2003) Dissociable contributions of the orbitofrontal and infralimbic cortex to pavlovian autoshaping and discrimination reversal learning: further evidence for the functional heterogeneity of the rodent frontal cortex. *J. Neurosci.*, **23**, 8771–8780.
- Cohen, J.Y., Haesler, S., Vong, L., Lowell, B.B. & Uchida, N. (2012) Neuron-type-specific signals for reward and punishment in the ventral tegmental area. *Nature*, **482**, 85–88.
- Cohen, J.Y., Amoroso, M.W. & Uchida, N. (2015) Serotonergic neurons signal reward and punishment on multiple timescales. *eLife*, **4**, e06346.
- Dalley, J.W., Everitt, B.J. & Robbins, T.W. (2011) Impulsivity, compulsivity, and top-down cognitive control. *Neuron*, **69**, 680–694.
- Fonseca, M.S., Murakami, M. & Mainen, Z.F. (2015) Activation of dorsal raphe serotonergic neurons promotes waiting but is not reinforcing. *Curr. Biol.*, **25**, 306–315.
- Howe, M.W., Tierney, P.L., Sandberg, S.G., Phillips, P.E. & Graybiel, A.M. (2013) Prolonged dopamine signalling in striatum signals proximity and value of distant rewards. *Nature*, **500**, 575–579.
- Izquierdo, A. & Murray, E.A. (2004) Combined unilateral lesions of the amygdala and orbital prefrontal cortex impair affective processing in rhesus monkeys. *J. Neurophysiol.*, **91**, 2023–2039.
- Jones, J.L., Esber, G.R., McDannald, M.A., Gruber, A.J., Hernandez, A., Mirenzi, A. & Schoenbaum, G. (2012) Orbitofrontal cortex supports behavior and learning using inferred but not cached values. *Science*, **338**, 953–956.
- Kazama, A. & Bachevalier, J. (2009) Selective aspiration or neurotoxic lesions of orbital frontal areas 11 and 13 spared monkeys' performance on the object discrimination reversal task. *J. Neurosci.*, **29**, 2794–2804.
- Kepcs, A., Uchida, N., Zarwala, H.A. & Mainen, Z.F. (2008) Neural correlates, computation and behavioural impact of decision confidence. *Nature*, **455**, 227–231.
- Knoch, D. & Fehr, E. (2007) Resisting the power of temptations: the right prefrontal cortex and self-control. *Ann. N. Y. Acad. Sci.*, **1104**, 123–134.
- Kringelbach, M.L., O'Doherty, J., Rolls, E.T. & Andrews, C. (2003) Activation of the human orbitofrontal cortex to a liquid food stimulus is correlated with its subjective pleasantness. *Cereb. Cortex*, **13**, 1064–1071.
- Lak, A., Costa, G.M., Romberg, E., Koulakov, A.A., Mainen, Z.F. & Kepcs, A. (2014) Orbitofrontal cortex is required for optimal waiting based on decision confidence. *Neuron*, **84**, 190–201.
- Liu, D., Gu, X., Zhu, J., Zhang, X., Han, Z., Yan, W., Cheng, Q., Hao, J. et al. (2014) Medial prefrontal activity during delay period contributes to learning of a working memory task. *Science*, **346**, 458–463.
- Ljubojević, V., Luu, P. & De Rosa, E. (2014) Cholinergic contributions to supramodal attentional processes in rats. *J. Neurosci.*, **34**, 2264–2275.
- Lucantonio, F., Takahashi, Y.K., Hoffman, A.F., Chang, C.Y., Bali-Chaudhary, S., Shaham, Y., Lupica, C.R. & Schoenbaum, G. (2014) Orbitofrontal activation restores insight lost after cocaine use. *Nat. Neurosci.*, **17**, 1092–1099.
- Mansouri, F.A., Buckley, M.J. & Tanaka, K. (2014) The essential role of primate orbitofrontal cortex in conflict-induced executive control adjustment. *J. Neurosci.*, **34**, 11016–11031.
- Mar, A.C., Walker, A.L., Theobald, D.E., Eagle, D.M. & Robbins, T.W. (2011) Dissociable effects of lesions to orbitofrontal cortex subregions on impulsive choice in the rat. *J. Neurosci.*, **31**, 6398–6404.
- Mariano, T.Y., Bannerman, D.M., McHugh, S.B., Preston, T.J., Rudebeck, P.H., Rudebeck, S.R., Rawlins, J.N., Walton, M.E. et al. (2009) Impulsive choice in hippocampal but not orbitofrontal cortex-lesioned rats on a non-spatial decision-making maze task. *Eur. J. Neurosci.*, **30**, 472–484.
- McAlonan, K. & Brown, V.J. (2003) Orbital prefrontal cortex mediates reversal learning and not attentional set shifting in the rat. *Behav. Brain Res.*, **146**, 97–103.
- McClure, S.M., Ericson, K.M., Laibson, D.I., Loewenstein, G. & Cohen, J.D. (2007) Time discounting for primary rewards. *J. Neurosci.*, **27**, 5796–5804.
- McDannald, M.A. (2015) Serotonin: waiting but not rewarding. *Curr. Biol.*, **25**, R103–R104.
- McGuire, J.T. & Kable, J.W. (2012) Decision makers calibrate behavioral persistence on the basis of time-interval experience. *Cognition*, **124**, 216–226.
- McGuire, J.T. & Kable, J.W. (2013) Rational temporal predictions can underlie apparent failures to delay gratification. *Psychol. Rev.*, **120**, 395–410.
- Menegas, W., Bergan, J.F., Ogawa, S.K., Isogai, Y., Umadevi Venkataraju, K., Osten, P., Uchida, N. & Watabe-Uchida, M. (2015) Dopamine neurons projecting to the posterior striatum form an anatomically distinct subclass. *eLife*, **4**, e10032.
- Miyazaki, K., Miyazaki, K.W. & Doya, K. (2011) Activation of dorsal raphe serotonin neurons underlies waiting for delayed rewards. *J. Neurosci.*, **31**, 469–479.
- Miyazaki, K.W., Miyazaki, K. & Doya, K. (2012) Activation of dorsal raphe serotonin neurons is necessary for waiting for delayed rewards. *J. Neurosci.*, **32**, 10451–10457.
- Miyazaki, K.W., Miyazaki, K., Tanaka, K.F., Yamanaka, A., Takahashi, A., Tabuchi, S. & Doya, K. (2014) Optogenetic activation of dorsal raphe serotonin neurons enhances patience for future rewards. *Curr. Biol.*, **24**, 2033–2040.
- Mobini, S., Body, S., Ho, M.Y., Bradshaw, C.M., Szabadi, E., Deakin, J.F. & Anderson, I.M. (2002) Effects of lesions of the orbitofrontal cortex on sensitivity to delayed and probabilistic reinforcement. *Psychopharmacology*, **160**, 290–298.
- Murakami, M., Vicente, M.I., Costa, G.M. & Mainen, Z.F. (2014) Neural antecedents of self-initiated actions in secondary motor cortex. *Nat. Neurosci.*, **17**, 1574–1582.
- Murphy, E.R., Dalley, J.W. & Robbins, T.W. (2005) Local glutamate receptor antagonism in the rat prefrontal cortex disrupts response inhibition in a visuospatial attentional task. *Psychopharmacology*, **179**, 99–107.
- Murphy, E.R., Fernando, A.B., Urcelay, G.P., Robinson, E.S., Mar, A.C., Theobald, D.E., Dalley, J.W. & Robbins, T.W. (2012) Impulsive behaviour induced by both NMDA receptor antagonism and GABA_A receptor activation in rat ventromedial prefrontal cortex. *Psychopharmacology*, **219**, 401–410.
- Padoa-Schioppa, C. & Assad, J.A. (2006) Neurons in the orbitofrontal cortex encode economic value. *Nature*, **441**, 223–226.
- Pattij, T. & Vandervschuren, L.J. (2008) The neuropharmacology of impulsive behaviour. *Trends Pharmacol. Sci.*, **29**, 192–199.
- Rabinovich, M., Huerta, R. & Laurent, G. (2008) Neuroscience. Transient dynamics for neural processing. *Science*, **321**, 48–50.
- Raposo, D., Kaufman, M.T. & Churchland, A.K. (2014) A category-free neural population supports evolving demands during decision-making. *Nat. Neurosci.*, **17**, 1784–1792.
- Rempel-Clower, N.L. (2007) Role of orbitofrontal cortex connections in emotion. *Ann. N. Y. Acad. Sci.*, **1121**, 72–86.

- Reyna, V.F. & Farley, F. (2006) Risk and rationality in adolescent decision making: implications for theory, practice, and public policy. *Psychol. Sci. Public Interest*, **7**, 1–44.
- Robbins, T.W. (2002) The 5-choice serial reaction time task: behavioural pharmacology and functional neurochemistry. *Psychopharmacology*, **163**, 362–380.
- Roesch, M.R., Taylor, A.R. & Schoenbaum, G. (2006) Encoding of time-discounted rewards in orbitofrontal cortex is independent of value representation. *Neuron*, **51**, 509–520.
- Roesch, M.R., Singh, T., Brown, P.L., Mullins, S.E. & Schoenbaum, G. (2009) Ventral striatal neurons encode the value of the chosen action in rats deciding between differently delayed or sized rewards. *J. Neurosci.*, **29**, 13365–13376.
- Roesch, M.R., Bryden, D.W., Cerri, D.H., Haney, Z.R. & Schoenbaum, G. (2012) Willingness to wait and altered encoding of time-discounted reward in the orbitofrontal cortex with normal aging. *J. Neurosci.*, **32**, 5525–5533.
- Rudebeck, P.H. & Murray, E.A. (2014) The orbitofrontal oracle: cortical mechanisms for the prediction and evaluation of specific behavioral outcomes. *Neuron*, **84**, 1143–1156.
- Rudebeck, P.H., Walton, M.E., Smyth, A.N., Bannerman, D.M. & Rushworth, M.F. (2006) Separate neural pathways process different decision costs. *Nat. Neurosci.*, **9**, 1161–1168.
- Rudebeck, P.H., Saunders, R.C., Prescott, A.T., Chau, L.S. & Murray, E.A. (2013) Prefrontal mechanisms of behavioral flexibility, emotion regulation and value updating. *Nat. Neurosci.*, **16**, 1140–1145.
- Schoenbaum, G., Setlow, B., Nugent, S.L., Saddoris, M.P. & Gallagher, M. (2003) Lesions of orbitofrontal cortex and basolateral amygdala complex disrupt acquisition of odor-guided discriminations and reversals. *Learn. Memory*, **10**, 129–140.
- Schoenbaum, G., Takahashi, Y., Liu, T.L. & McDannald, M.A. (2011) Does the orbitofrontal cortex signal value? *Ann. N. Y. Acad. Sci.*, **1239**, 87–99.
- Stalnaker, T.A., Cooch, N.K. & Schoenbaum, G. (2015) What the orbitofrontal cortex does not do. *Nat. Neurosci.*, **18**, 620–627.
- Wallis, J.D. (2007) Orbitofrontal cortex and its contribution to decision-making. *Annu. Rev. Neurosci.*, **30**, 31–56.
- Winstanley, C.A., Theobald, D.E., Cardinal, R.N. & Robbins, T.W. (2004) Contrasting roles of basolateral amygdala and orbitofrontal cortex in impulsive choice. *J. Neurosci.*, **24**, 4718–4722.
- Zeeb, F.D., Floresco, S.B. & Winstanley, C.A. (2010) Contributions of the orbitofrontal cortex to impulsive choice: interactions with basal levels of impulsivity, dopamine signalling, and reward-related cues. *Psychopharmacology*, **211**, 87–98.
- Zelikowsky, M., Bissiere, S., Hast, T.A., Bennett, R.Z., Abdipranoto, A., Vissel, B. & Fanselow, M.S. (2013) Prefrontal microcircuit underlies contextual learning after hippocampal loss. *Proc. Natl. Acad. Sci. USA*, **110**, 9938–9943.
- Zhou, J., Jia, C., Feng, Q., Bao, J. & Luo, M. (2015) Prospective coding of dorsal raphe reward signals by the orbitofrontal cortex. *J. Neurosci.*, **35**, 2717–2730.